AFWAL-TR-81-4019
Volume II

COMPUTER MODELING OF TITANIUM COMBUSTION

M. R. Glickstein
Pratt & Whitney Aircraft Group
Government Products Division
West Palm Beach, Florida

ABSTRACT

Titanium and its alloys are known to undergo self-sustained combustion when ignited in aerodynamic environments. Energy in several forms, i.e., radiation, frictional heating, or aerodynamic heating can be sufficient to bring the material to the condition where self-sustained combustion can occur. This phenomenon is of interest in the aircraft industry because of the extensive use of titanium in aircraft propulsion systems.

An extensive program of analytical and experimental investigation has been in progress for the past four years to establish the parameters that govern the ignition and self-sustained combustion of titanium in propulsion system environments. An analytical model is being evolved to predict this ignition and subsequent propagation of combustion of titanium alloys. The model uses finite-element and time-marching techniques to produce simultaneous solutions of the equations governing heat and mass transfer in the aerodynamic boundary layer, transient thermal conduction in the solid metal, phase change and liquid metal flow over the solid surface. Appropriate models describe the oxidation kinetics at the metal surface, flow of liquid metal due to aerodynamic shear and centrifugal body forces, and diffusion of oxides within the molten metal. The model allows prediction of metal ignition due to a variety of sources, i.e., radiation, frictional heating, and exposure to high ambient temperatures.

The analytical model and its development over the past three years is described, and an analytical simulation of a propagating fire is compared with experimental data.

INTRODUCTION

Titanium and titanium alloys are used extensively in aerospace systems because of their high strength-to-density ratio, temperature resistance and excellent corrosion behavior. Titanium alloys have been widely applied to aircraft structural components, and to turbine engine and compressor parts. As titanium alloys have found application in different environments, especially at increasingly higher temperatures and pressures, a renewed interest has developed in their ignition and combustion behavior in air.

Within the last ten years, the incidence of titanium fires in gas turbine engines has markedly increased. Most frequently, catastrophic massive-metal fires have been observed during test cell performance evaluations. A number of factors are involved in this trend; most notably, the increase in thrust-to-weight ratio of current engines. Lower weight demands a more flexible engine and lighter components and these factors, when added to the desire for more thrust, result in increased pressure, temperature and flow, providing an environment conducive to ignition, self-sustained combustion and propagation of a titanium fire.

To date, the primary remedy has involved substitution of steels for selected titanium parts, with a resultant weight penalty, and an increase in the rotor/stator clearances with a resulting performance penalty. As these penalties may be unacceptable in certain "performance-driven" military systems, the Air Force has initiated a program to understand the phenomena and develop materials approaches to eliminate catastrophic failure.

This program includes several studies to consider various types of ignition, such as rubbing or rapid heating, and to investigate and model self-sustained combustion of titanium alloys in the gas turbine engine compressor environment.

Glickstein, et al. (Reference 1), reported the early development of an analytical model to simulate the ignition and propagation of titanium fires on massive blade-like shapes in flowing gas. Given a rectangular or airfoil shaped titanium alloy specimen in a compressor environment, and sufficient energy for ignition at a corner or edge, several factors will determine whether propagation occurs. The combination of gas-temperature, pressure and velocity control the concentration of reactants at a combusting surface, the aerodynamic shear for removal of melted materials, and the convective cooling of the surface. No prior efforts have determined the dependence of ignition or propagation on these factors. The objective of this effort was to develop an understanding of the interrelationships of the importance factors governing ignition and combustion propagation over a broad range of environmental conditions.

Since the publication of Reference 1, development of the model has continued, evolving an analytical tool for predicting the fire sensitivity of titanium in a wide variety of aerodynamic applications.

ANALYTICAL MODEL

To provide a procedure for predicting the fire susceptibility of titanium structures in aerodynamic environments, an analytical model was developed based on experimental observations (Reference 1). This model, while considering most of the observed phenomena of a propagating fire, was somewhat limited in its treatment of certain details of the process, as evidenced by comparison with test data. Furthermore, it was not capable of treating rotating airfoils, with the added complexity of centrifugal forces combining with aerodynamic shear forces in causing the removal of molten material.

In order to clarify the relationship of combustion rates, total damage and ignition, it is important to consider the entire ignition-propagation sequence with regard to the local environment. Based on observation of high speed movies and applied to a gas turbine engine environment, the following scenario can be developed to describe the titanium fire phenomena: A titanium specimen is exposed to and is in thermal equilibrium with an aerodynamic environment. Heat generated by

normal oxidation is balanced by losses to the surrounding environment. An ignition initiation event creates an imbalance in this equilibrium system. Such an event may take one of several forms, i.e., heat input due to mechanical friction, thermal radiation, aerodynamic heating or fracture which produces an atomically fresh surface. In response to one of these events, metal temperature increases in the region of heat input, resulting in increased heat generation from oxidation. Heat loss to the environment and to the sample increases accordingly to establish a new equilibrium state. If thermal equilibrium is reached with the local metal surface temperature below its melting point, ignition does not occur, and the system returns to its original state when the ignition source is removed. If melting occurs, the material ignites and, with removal of the ignition source, may cease burning if the thermal balance is insufficient to supply the necessary latent heat to continue local melting. If the rate of local heat generation is greater than the rate of losses, self-sustained combustion occurs. In the case of self-sustained combustion and subsequent propagation, test results demonstrate that a significant amount of molten material is generated at the leading edge of the specimen and adheres to and flows over the surface in response to aerodynamic forces. This flowing liquid, with considerable dissolved oxygen, continues to react as it flows, thereby maintaining its liquid state and providing additional energy to the specimen by conduction. The adherence of this molten metal in certain environments is critical to the maintenance of self-sustained combustion, and is the principal mechanism for propagation of titanium combustion at moderate-to-great airstream velocities. In general, the transport of energy along the surface in the molten flow far exceeds the capability for heat loss by conduction with the solid substrate. A more accurate description of this process must come from analytical modelling.

A. The Physical System

Figure 1 illustrates a compressor rotor blade with ignition at the airfoil leading edge and fire propagation across the blade surface. This figure shows the salient features of the process, with molten metal streaming from the leading edge of the burning zone to the downstream edge of the "melt" region, henceforth called the melt leading edge. The aerodynamic leading edge is called the stagnation region.

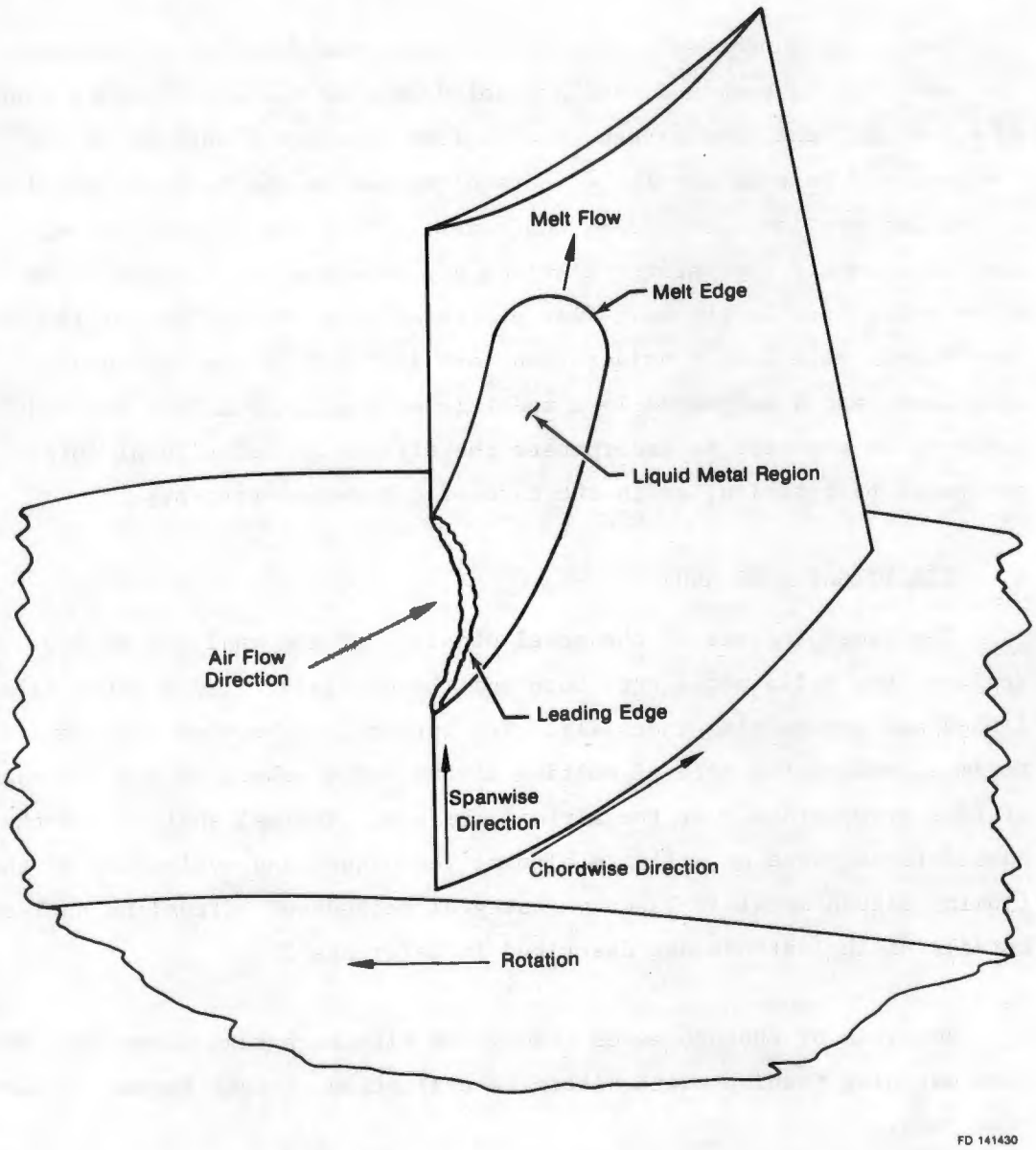

Figure 1. Features of a Burning Compressor Rotor Blade

Comparison of liquid metal velocities, evaluated from photographic data, with thermal diffusion rates in the solid airfoil substrate indicate that liquid metal flow is the primary mode of thermal propagation in a buring airfoil.

In the refined model, described herein, the detailed structure of the melt flow is examined, and a model developed for simultaneous transport of momentum, heat, and oxygen species from the liquid surface to the liquid-solid interface. The effects of oxides on the relevant physical properties are incorporated in the model, within the limitations of available data. Continuity relations are developed in integral form to allow evaluation of the melt flow processes over the surface of the airfoil. Aerodynamic melt loss considerations are included in the continuity equations, and a suggested loss model is proposed. Finally, the model geometry is expanded to incorporate the effects of centrifugal forces generated by rotation, as in the case of compressor rotors.

B. ANALYTICAL APPROACH

The gross feature of the model consists of the analysis of two regimes, the solid metal structure and the overlying liquid metal film, linked and interacting thermally. The interaction between these two regimes governs the rate of melting of the solid substrate and the rate of fire propagation over the airfoil surface. Thermal analysis of the substrate is based on a finite element technique, and evaluation of the flowing liquid metal is based on integral methods of streamline analysis. Details of the methods are described in Reference 2.

Analysis of the processes associated with each regime proceeds in a time marching fashion, with alternate evaluation of each regime at each time step.

Energy enters the system from external sources (convection, radiation, mechanical friction) or is generated by reaction at the air-metal interface. The principle reactions in the titanium-oxygen system are assumed to occur at the metal-gas interface. Energy is lost from the burning surface by

convection and radiation to the surroundings, and by conduction into the substrate. The net balance of these energy flows governs the rate of melting of the solid substrate.

The reaction rate at the metal surface, either as slow oxidation or as rapid combustion, is governed by the rate at which oxygen can flow from the air to the surface and bond with free metal in the substrate. The overall process is governed by the most restrictive step in the foregoing chain of events. The most restrictive step is dependent on the surface temperature, amount of surface oxides, and the nature of the boundary layer mass diffusion process.

The governing process is assumed to be the most restrictive of the following: (1) oxygen diffusion through the surface oxides at low temperature (parabolic kinetics), dependent on surface temperature and amount of accumulated oxides, (2) linear kinetics at high temperatures, dependent on surface temperature only, or (3) oxygen diffusion rate through the aerodynamic boundary layer.

Parabolic or linear kinetics are assumed to occur on the solid surfaces, but based on experimental observations, the rate controlling process during combustion appears to be oxygen diffusion through the aerodynamic boundary layer. The details of the assumed kinetics are described in References 1 and 2.

The corresponding reaction rate at the surface is:

$$g_r = H_\infty \frac{dM}{dt} \qquad (1)$$

where H_∞ is the heat of reaction per mass of oxygen, based on the reaction assumed to occur at a particular condition. Post-test analysis of burned airfoil specimens indicated the primary reaction product resulting from slow oxidation is TiO_2 while rapid combustion results in approximately equal weights of TiO and Ti_3O_5. The corresponding heats of reaction have been incorporated in the model, i.e., TiO_2 is assumed to result from solid surface oxidation, while 50% TiO-Ti_3O_5 is assumed to result when combustion occurs on a molten surface.

C. Thermophysical Properties

The physical properties of titanium relevant to the overall combustion model include the thermodynamic properties, defining the state and internal energy, and the transport properties, defining the rate of the various transport processes. These properties in general are dependent on the metal temperature, alloying elements and amount of oxygen present, and the crystalline structure. Because of insufficient data, the present analysis has not included alloying effects, but has as far as possible included the effect of temperature, phase, and oxygen content. The effect of temperature and oxygen content are considered in evaluating the melt viscosity and thermodynamic state, and the effect of temperature is considered on the thermal conductivity and oxygen diffusivity.

Figure 2 shows a phase diagram for the titanium-oxygen system, developed by Schofield and Bacon (Reference 3). Oxygen in titanium is seen to act as a phase stabilizer resulting in the occurrence of α-Ti at temperatures above the normal α-β transition, and increasing the liquidus temperature significantly. It is further noted that the presence of dissolved oxygen causes the occurrence of a solidus-liquidus temperature range, or two-phase region, at low concentrations.

A corresponding thermodynamic phase diagram was constructed, based on thermodynamic data for pure titanium (Reference 3).

The presence of oxygen is assumed to act only as a phase-stabilizer causing the effect of the energy of α-β transition to be shifted to the melting temperature range. While the resulting enthalpy diagram, shown in Figure 3, may not be entirely correct, it provides a workable basis for modeling the heat transfer through the melt flow.

The net effect of oxygen diffusion into the liquid film is to produce a thickened suspension of solid particles in the outer region of the film. The suspending liquid retains the properties of pure liquid at the equilibrium temperature, and the overall effect of the suspended solids is an increase in the viscosity. Basing the viscosity of the liquid on the data

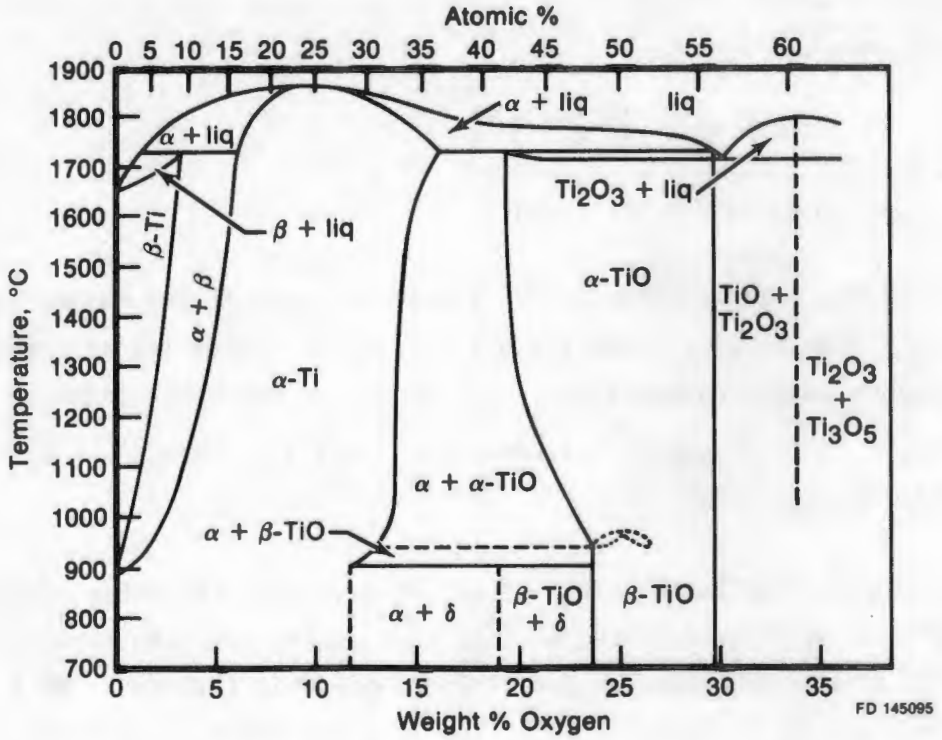

Figure 2. The Ti-O Phase Diagram Up to 35 Wt % Oxygen After Schofield and Bacon

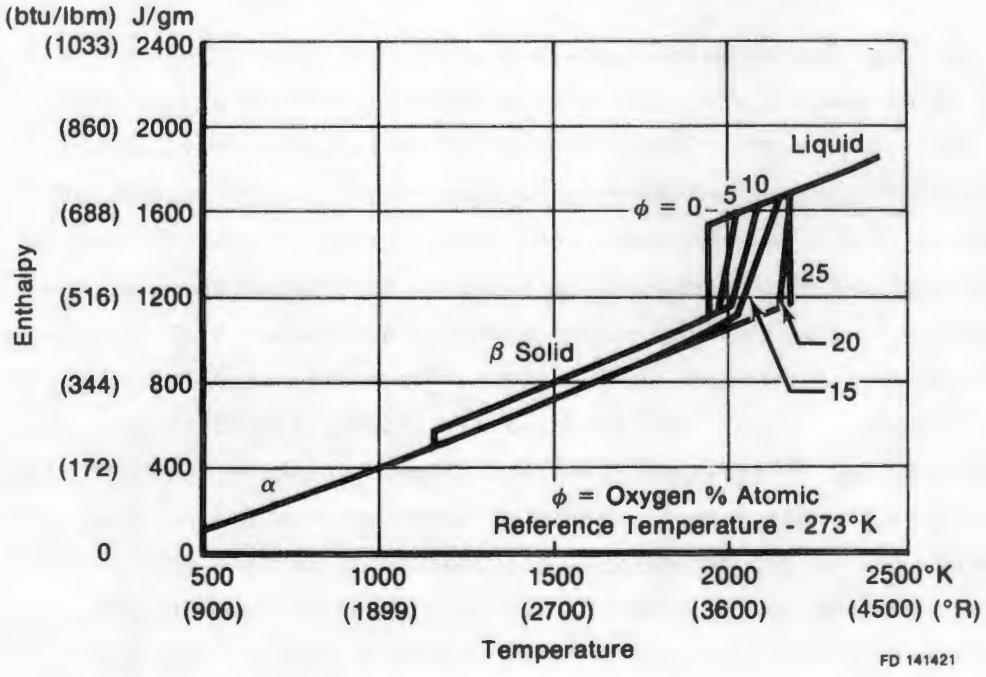

Figure 3. Enthalpy of Titanium-Oxygen System as Function of Temperature

of Orr (Reference 5), a model for the viscosity of molten two-phase titanium takes the form:

$$\frac{\mu_1}{\mu_0} = \frac{\left[1 - 2.86 \left(\frac{H_{s_1} - H_1}{H_{s_1} - H_{\ell_1}} \right) \right]^{-1.8}}{\left[1 + 7.54 \times 10^{-3} (T_1 - T_0) \right]} \qquad (1)$$

where μ_o is the dynamic viscosity of liquid titanium in the oxygen-free condition at the melting temperature T_o, μ_1 is the voscosity at temperature T_1 and oxygen concentration ϕ_1 (H_1, H_{ℓ_1}, H_{s_1}) are the enthalpies at concentration ϕ_1 and respective temperature T_{ℓ_1} and T_{s_1}, liquidus temperature and solidus temperature.

Data is not available on the effect of oxygen on the other transport properties in the liquid state, nor for that matter for pure titanium in the liquid state. The data of Roe, Palmer, and Opie (Reference 6) for oxygen diffusivity in titanium is extrapolated to the melting temperature, and treated as temperature dependent only. The data of Touloukian (Reference 7) for thermal conductivity is treated in the same manner.

D. Structure of the Melt Flow

In the flowing melt region a liquid layer of thickness δ is assumed to flow on the surface, driven by aerodynamic forces in the direction of air flow, and by centrifugal forces in the radial outward direction. Oxygen flows in the aerodynamic boundary layer to the liquid surface, reacts with the melt, and the resulting heat and oxides diffuse into the melt layer. Shear stress across the melt is assumed constant, and momentum transport is considered small by comparison. Figure 4 illustrates the features of the flowing liquid layer. The coordinates (x, y, z) are in the chordwise, normal, and spanwise directions, respectively. The velocity components (u, v) represent the local liquid velocity in the two surface directions and are seen to vary with distance from the surface. The temperature and oxygen concentration at the outer surface are T_1 and ϕ_1, and at the inner surface are T_o and ϕ_o. Oxygen flows into the melt layer at a rate $\dot{m}_o$, and the liquid-solid interface recedes or advances (melting or solidification) at a velocity U.

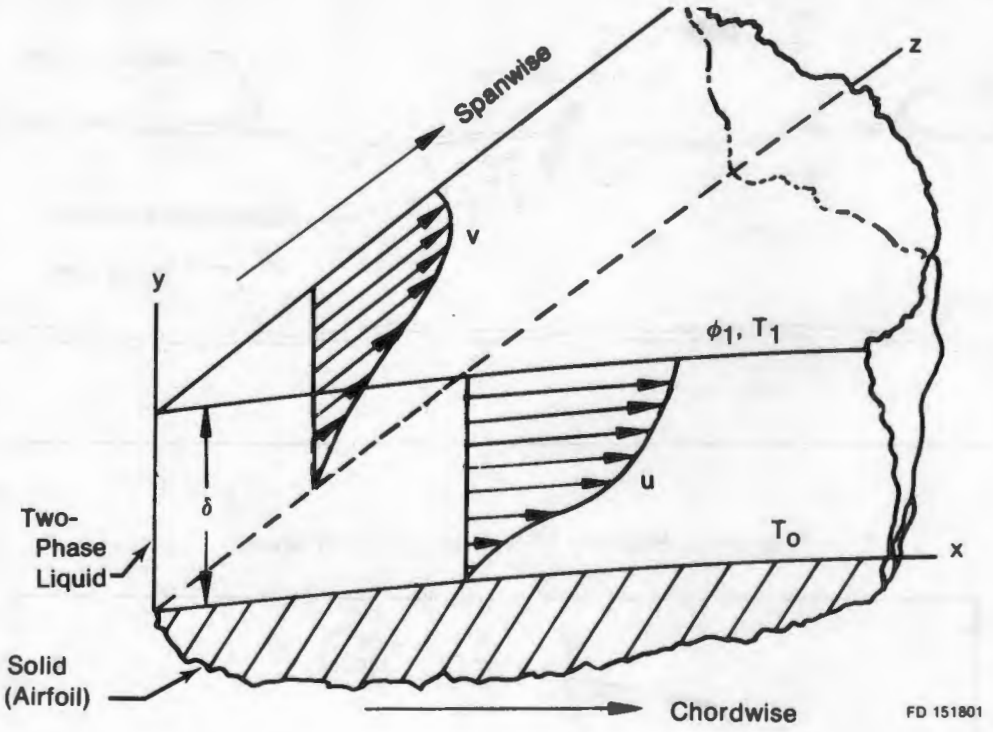

Figure 4. Features of Liquid Flow Model

Melting is assumed to occur at the solid-liquid interface in the oxygen-free state. Diffusion of oxygen into the liquid from the reaction surface results in the precipitation (re-solidification) of oxygen-rich titanium from the melt, as shown in Figure 5. Thermodynamic and phase-equilibria are assumed during this process.

The solidified material is assumed to occur in distributed particulate form, in thermal equilibrium with the oxygen-free liquid. Figures 6 and 7 show the thermodynamic and phase relations of the state points defined in Figure 5. States (a) and (b) correspond to oxygen-free titanium, and (c) is the condition at the air-melt interface. In Figure 6, state C corresponds to the condition in the melt at the air-melt interface if there were no oxygen diffusion. The temperature at C' is T'_1, determined by one-dimensional conduction without heat sinks. Solidification is assumed to be a net constant energy process, i.e., the local enthalpy of the liquid-solid system remains constant as solids precipitate. Solids and liquid are in local thermal equilibrium and the solidification process

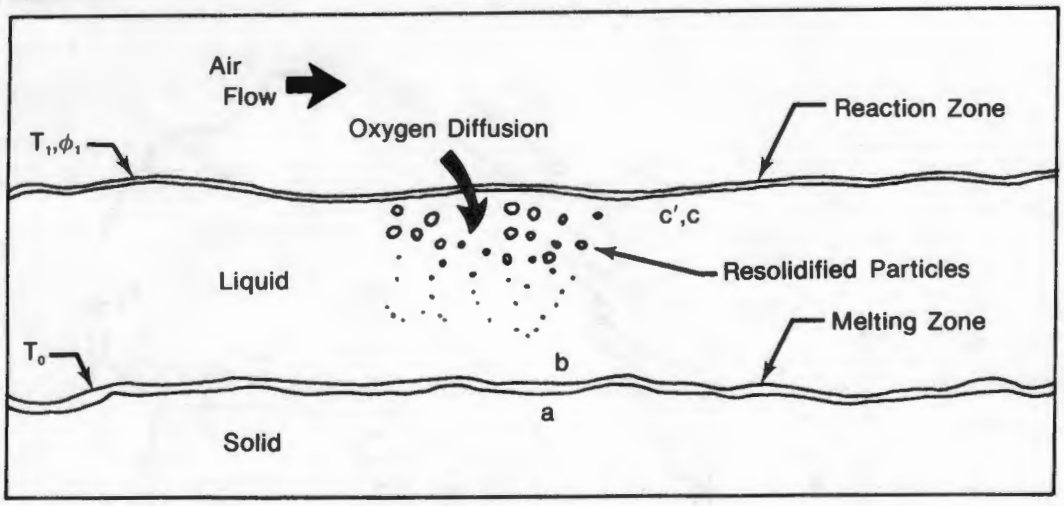

Figure 5. Features of Melting-Diffusion Model

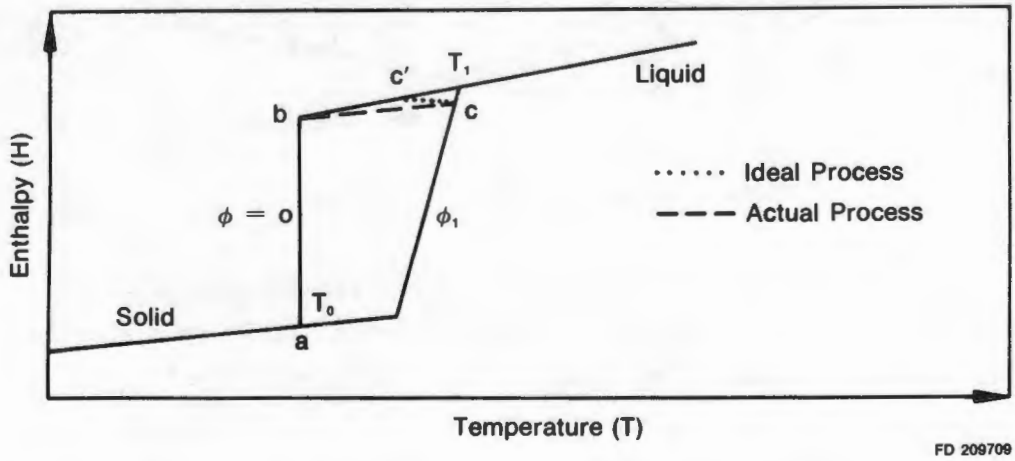

Figure 6. Thermodynamic Model of Melting-Diffusion Process

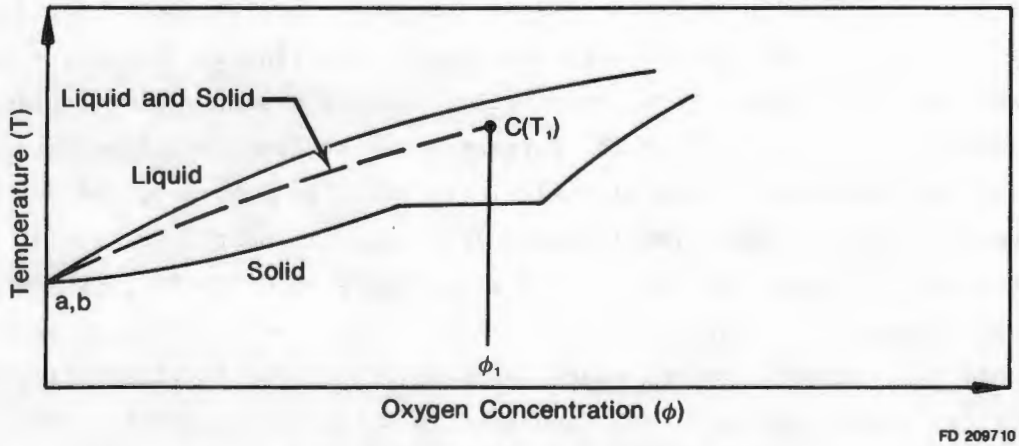

Figure 7. Phase Model of Melting-Diffusion Process

is accompanied by an increase in temperature due to release of the heat of fusion. The idealized process path is C'-C, in Figure 6. The final equilibrium temperature at state C is T_1.

E. INTEGRAL TRANSPORT EQUATIONS

In Figure 1 the melt region is illustrated with a single streamline. The melt flow field can be considered as composed of a set of streamlines originating in the stagnation region and ending at the downstream edge of the melt region, as shown in Figure 8. If a coordinate system is described by (S,J), where S is the distance along the streamline and J is the streamline number, analysis of the melt flow can be performed along each streamline. Let the liquid flow rate in a streamline at a point (S,J) be $\rho\overline{F}$, then $\overline{F}$ is a vector quantity aligned in the direction of the streamline. The flow vector $\overline{F}$ can be described as composed of components (f) in the chordwise and (h) in the spanwise directions. Thus,

$$\overline{F} = if + jh \tag{2}$$

where i and j are unit vectors in the component directions. The direction of the streamline can be described by the angle (ψ) with the chord, where

$$\tan \psi = f/h \tag{3}$$

The melting airfoil adds to the streamline flow in the amount ρU per unit length of streamline. If the fraction of flow rate lost to the airstream is ξ per unit length, then the rate of change of flow in the streamline is

$$\frac{d\overline{F}}{ds} = \overline{s}U - \xi\overline{F} \tag{4}$$

where $\overline{s}$ is a unit vector in the direction of the streamline, and the derivative is taken in the direction of flow. This expression can also be written in terms of the flow components as:

$$\frac{df}{ds} = U \cos \psi - \xi f \tag{5a}$$

$$\frac{dh}{ds} = U \sin \psi - \xi h \tag{5b}$$

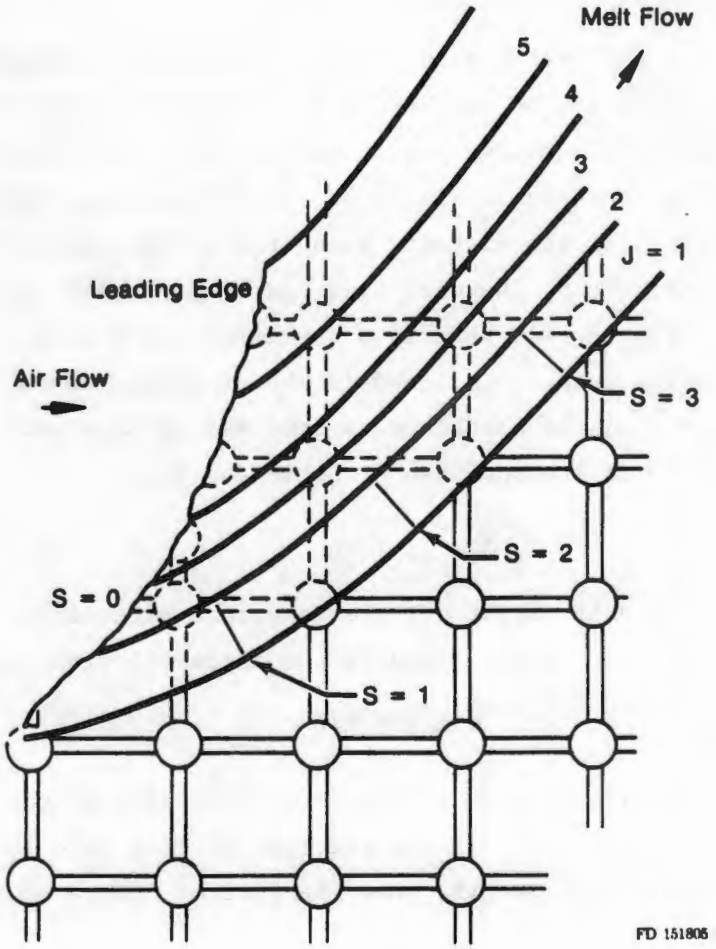

Figure 8. Streamline Coordinate System

In a similar fashion, the flow rate of oxygen carried along the surface by the melt is (g), and is related to the melt flow by

$$g = \rho F \bar{\phi} \tag{6}$$

where

$$F = \sqrt{f^2 + h^2}, \tag{6}$$

and $\bar{\phi}$ is the local bulk concentration of oxygen in the melt.

The rate of change of g along the surface is given by:

$$\frac{dg}{ds} = \dot{m}_o - \xi \phi_1 \rho F \tag{7}$$

The concentration at the liquid surface (ϕ_1) is presumed to describe the average concentration of the melt loss at the surface.

The set of equations (5a, b) and (7), describe the change in liquid mass flow and oxygen content of the streamlines as they flow over the surface.

F. Local Transport Processes

Integration of the integral transport equations requires evaluation of the initial conditions, i.e., values of (f, h, g) at the stagnation point. In addition, these transport functions must be related to the local transport processes to allow evaluation of the physical variables, such as local velocity, temperature, and concentration.

1. Axial (Chordwise) Velocity Profile

The melt flow is assumed to be laminar, with constant shear stress, and with no slip at the liquid-solid interface. Assuming the velocity profile to be represented by a second degree equation:

$$u = a + b\eta + c\eta^2 \tag{8}$$

where

$$\eta = y/\delta$$

The shear stress τ, must be equal to the aerodynamic shear, determined from boundary layer analysis, and is related to the velocity profile by:

$$\tau = \frac{\mu_0}{\delta}\frac{du}{d\eta}\Big|_{y=0} = \frac{\mu_1}{\delta}\frac{du}{d\eta}\Big|_{y=\delta} \tag{9}$$

where subscripts '1' and '0' refer to evaluation at conditions at the liquid and solid surfaces. With the no-slip conditions (u = 0, y = 0) and Equation (9), the constants in Equation 8 can be determined, yielding the velocity equation:

$$u(\eta) = \frac{\tau\delta}{\mu_0}\eta + \frac{\tau\delta}{2\mu_0}\left(\frac{\mu_0}{\mu_1} - 1\right)\eta^2 \tag{10}$$

The axial component of flow in the streamline (per unit width is:

$$\rho f = \int_0^\delta \rho u dy = \frac{\rho\delta^2\tau}{\mu_0}\int_0^1 \left[\eta + \frac{1}{2}\left(\frac{\mu_0}{\mu_1} - 1\right)\eta^2\right] d\eta \tag{11}$$

Hence

$$f = \frac{\tau\delta^2}{6\mu_0}\left[\frac{\mu_0}{\mu_1} + 2\right] \tag{12}$$

2. Radial Velocity Component

Fluid motion in the radial direction is driven by centrifugal body force (β), and resisted by aerodynamic shear stress (τ_0) due to the motion of the liquid relative to the air stream. A simple analysis, balancing radial forces, shows that the shear stress generated by body forces varies linearly from the liquid surface to a maximum at the solid surface. The aerodynamic shear stress is found to be constant across the melt. The total stress is:

$$\tau = \beta\delta(1-\eta) - \tau_0 \tag{13}$$

where

$$\beta = \rho \bar{R} \omega^2 \quad \text{and} \quad \tau_0 = C_f \frac{\rho_a v_i^2}{2} \tag{14}$$

The centrifugal force depends on the radius to the blade midspan ($\bar{R}$) and the rotational speed (ω) of the compressor stage. The aerodynamic shear stress, is a function of the local friction coefficient (C_f) and the relative liquid velocity at the air-liquid interface (v_1). Approximating the velocity profile by a second degree polynomial,

$$v(\eta) = a + b\eta + c\eta^2 \tag{15}$$

the laminar relation between shear stress and velocity gradient is combined with Equation 13 and integrated to yield the velocity profile:

$$v(\eta) = \frac{\beta \delta^2}{\mu_0} \left[\eta - \frac{\eta^2}{2} \right] - \frac{\tau_0 \delta}{\mu_0} \left[\eta - \frac{1}{2} \left(\frac{\mu_0}{\mu_1} - 1 \right) \eta^2 \right] \tag{16}$$

the surface velocity (v_1) is determined by combining Equations 14 and 16, for $\eta = 1$, yielding:

$$v_1 = \frac{-1 + \sqrt{1 + \rho_a C_f \beta \delta^3 \left(\frac{\mu_0}{\mu_1} + 1 \right)}}{\frac{\rho_a \delta C_f \left(\frac{\mu_0}{\mu_1} + 1 \right)}{2 \mu_0}} \tag{17}$$

The radial flow component is now calculated in the same manner as the axial component, resulting in the relation:

$$h = \frac{\beta \delta^3}{3\mu_0} - \frac{\tau_0 \delta^2}{6\mu_0} \left(\frac{\mu_0}{\mu_1} + 2 \right) \tag{18}$$

3. Oxygen Concentration Profile

The distribution of oxygen mass function (ϕ) is assumed to be a third order power function of the distance from the solid surface:

$$\phi(\eta) = a + b\eta + c\eta^2 + d\eta^3 \tag{19}$$

The coefficients are evaluated by satisfying the following conditions at the solid and liquid surfaces:

a. Flow rate of oxygen into the liquid surface is equal to the diffusion rate into the melt.

b. Diffusion rate in the liquid goes to zero at the solid-liquid interface.

c. The oxygen concentrations in the liquid and solid are zero at the interface.

The resulting concentration profile must be related to a reference value. Relating to the liquid surface:

$$\phi(\eta) = (3\phi_1 - \Gamma)\,\eta^2 + (\Gamma - 2\,\phi_1)\,\eta^3 \qquad (20)$$

where $\Gamma = \delta\,\dot{m}_0/\rho\,D_1$, and D_1 is the oxygen diffusivity at the surface temperature T_1.

The bulk concentration, $(\overline{\phi})$, is obtained by integration of the product of the velocity and concentration profiles:

$$\overline{\phi} = \frac{\int_0^1 \phi\overline{V}d\eta}{\int_0^1 \overline{V}d\eta} \qquad (21)$$

where $\overline{V}$ is the liquid velocity vector. Combining Equations 10, 16, and 20, and performing the integration indication indicated in 21 yields a relationship between the bulk and liquid surface concentrations $(\overline{\phi},\ \phi_1)$. The surface concentration is the positive root of the following quadratic equation:

$$F_1\,\phi_1^2 - 2F_2\,\Gamma\,\phi_1 + 2\,\Gamma^2 - 100\,\overline{\phi}^2 = 0 \qquad (22)$$

where

$$F_1 = \left[\frac{13 + 8\psi}{2 + \psi} \right]^2 + \left[\frac{13B - 13\pi - 8\pi\psi}{2B - 2\pi - \pi\psi} \right]^2$$

$$F_2 = \left[\frac{13 + 8\psi}{2 + \psi} \right] + \left[\frac{13B - 13\pi - 8\pi\psi}{2B - 2\pi - \pi\psi} \right]$$

$$B = \frac{\beta\delta}{\tau} \; ; \pi = \frac{\tau_o}{\tau} \; ; \psi = \frac{\mu_o}{\mu_1}$$

G. SURFACE MELTING RATE

Heat transfer into the flowing melt consists of the sum of several components, heat generation due to chemical reaction at the surface, discrete surface heat input (i.e., laser radiation), and convective and radiant exchange with the surrounding environment.

The net difference between these heat flows, and the heat flow into the solid substrate by conduction, determines the rate of melting of the substrate. Writing an energy equation for the solid-liquid interface in generalized vector form:

$$\rho H_{sl} \bar{U} = \bar{q}_s - \bar{q}_k \qquad (23)$$

where

$\bar{U}$ = velocity of melting surface

$\bar{q}_s$ = net surface heat flux normal to surface

$\bar{q}_k$ = conduction heat flux into solid substrate

H. STAGNATION REGION ANALYSIS

Integration of Equations 5 and 7, with evaluations of the corresponding local processes, defines the development of melt flow over the airfoil surface. However, this evaluation requires that conditions at the stagnation point be known to provide initial conditions for the integration. Specifically, these quantities are required to start the calculation, the melt thickness (δ), the bulk concentration ($\bar{\phi}$), and the melting velocity at the leading edge (U). Figure 9 shows a cross-sectional view of the leading edge with the relevant features.

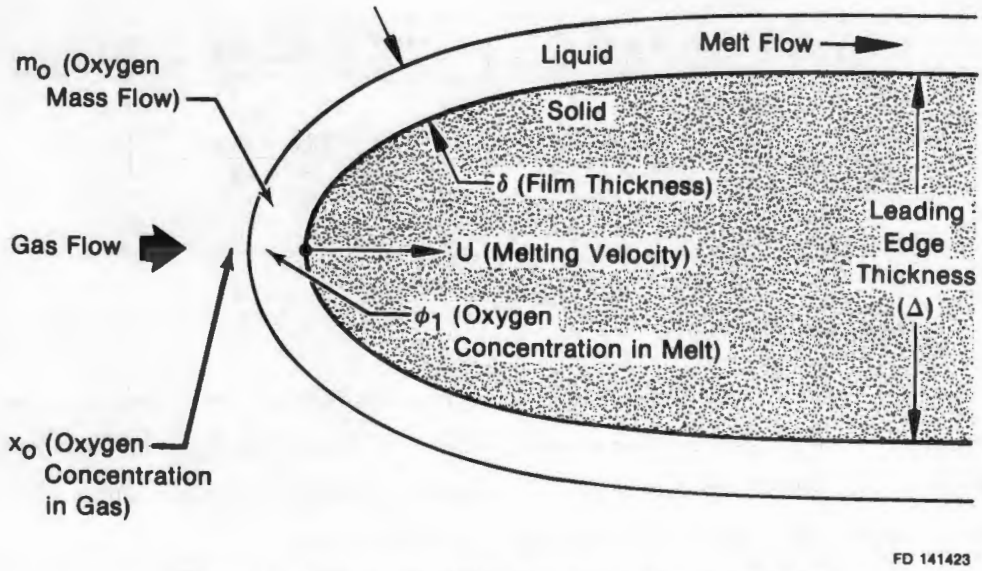

Figure 9. Stagnation Point Region of Burning Airfoil

Based on post-test examination of burned specimens, the cross-sectional shape of a melting leading edge will be considered an elliptic cylinder with an aspect ratio R (width/length).

The initial concentration is determined by expanding Equation 7, taking the limit as S→0, and noting that the aerodynamic shear stress vanishes at the stagnation point. This results in an expression for the bulk stagnation concentration:

$$\overline{\phi} = \frac{\dot{m}_o}{\rho U} \tag{24}$$

Consider the starting point for streamline (J=1) in Figure 8, noting that the leading edge is yawed to the direction of airflow. Figure 10 shows a large planform view of the leading edge and the relative directions of the various heat fluxes and the melting velocity.

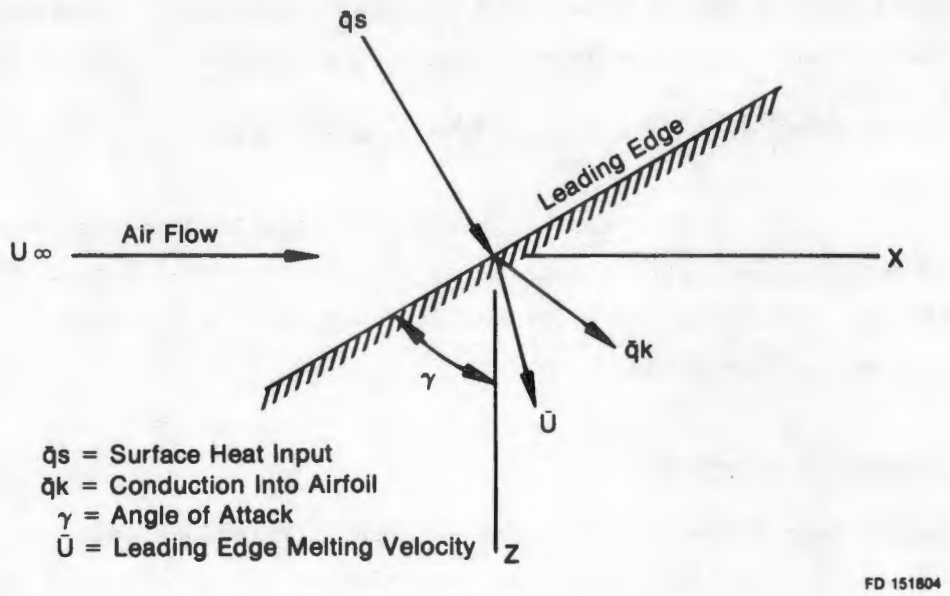

Figure 10. Heat Flow and Velocity Relationship at Burning Leading Edge

The leading edge is at a yaw angle (γ) to the airstream. The surface heat flux ($\bar{q}_s$) is normal to the leading edge, and the internal conduction flux ($\bar{q}_k$) points in the direction of maximum temperature gradient in the solid. The magnitude and direction of the melting velocity is determined by the vector addition defined in Equation 23. It is worthy of note that the melting velocity at the leading edge lies in the plane of the airfoil leading edge at an angle defined by the heat transfer. Over the remainder of the airfoil surface the melting velocity vector is oriented normal to the airfoil surface, since the surface and internal fluxes are aligned everywhere except at the leading edge. It is the effect of the internal conduction term in Equation 23 that controls the relative burning rates in the chordwise and spanwise directions, observed in the combustion tests.

The initial melt thickness is found by taking Equations 5a, b to the limit at the stagnation point. Writing these equations in terms of components normal to the leading edge, and considering the variation of aerodynamic shear stress and centrifugal force as the stagnation point is

approached, an expression is derived relating initial melt thickness to the other parameters at the leading edge. The resulting equation in (δ) is:

$$\frac{\delta^3 \beta \sin\gamma}{R\Delta} + \delta^2 \rho_\infty U^2 \infty \frac{d C_{fo}}{dn} \cos^2 \gamma = 12 \mu_1 U \tag{25}$$

where β is defined by Equation 14, R and Δ are the leading edge aspect ratio and thickness. The derivative of the friction coefficient is evaluated at the stagnation point and is found to be a function of R, Δ, and the leading edge Reynolds number.

I. STREAMLINE CONTINUITY

Independent analysis of flow in adjacent streamlines does not implicitly avoid continuity conflicts, such as intersection of streamlines. To ensure that continuity is satisfied, a condition of streamwise continuity is imposed on the solutions for streamline thickness. If the width of a streamline is (W), then continuity requires that (FW) be constant along the streamline, where F is the magnitude of the flow vector. This statement is expressed by:

$$\frac{d}{ds} W^2 (f^2 + h^2) = 0 \tag{26}$$

If local rates of changes of shear stress and body force are considered secondary, Equation 26 can be expanded into:

$$\frac{d\delta}{ds} = - \frac{\delta(f^2 + h^2) \frac{dW}{ds}}{W(2f^2 + 3h^2 + hf \frac{\tau_o}{\tau})} \tag{27}$$

This relation expresses the required correction in the calculated growth of the melt thickness necessary to satisfy streamline continuity.

J. MELT LEADING EDGE FLOW

Analysis of the motion of the liquid front (melt leading edge) over the solid structure requires considerations of the two-dimensional nature of the flow, including effects of both aerodynamic and body forces. Figure 11 shows the melt leading edge region isolated as a free body.

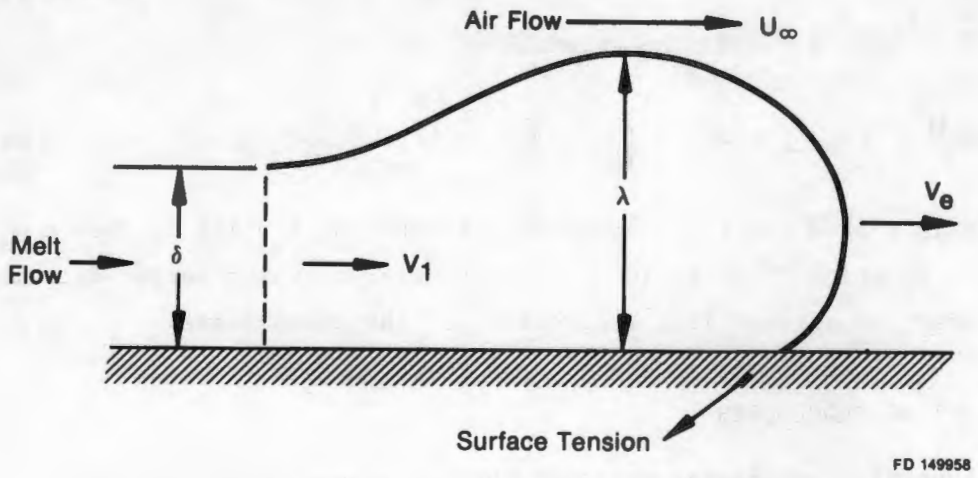

Figure 11. Leading Edge of Melt

The sum of forces acting on the fluid must be zero for steady motion. These forces include the aerodynamic drag force (F_D), the component of surface tension parallel to the solid surface (ζ), and the internal forces due to momentum change in the liquid as its velocity is reduced within the leading edge region (F_{int}). If the liquid velocity is V_1 as it approaches the leading edge zone, and the edge moves at an average velocity V_e, the internal force is equal to the liquid momentum change, or:

$$F_{int} = \dot{m} (V_1 - V_e) = \rho\delta V_1 (V_1 - V_e). \tag{28}$$

Considering continuity of flow

$$\rho\delta V_1 = \rho\lambda V_e = \rho F \tag{29}$$

where F is the magnitude of the flow vector defined in Equation 2. Combining these expressions.

$$F_{int} = \frac{\rho F^2}{\lambda} \left(\frac{\lambda}{\delta} - 1 \right) \tag{30}$$

The aerodynamic drag is

$$F_D = C_D \frac{\rho_a U_\infty^2}{2} \lambda \cos^2 \psi \tag{31}$$

Summation of forces yields the relation

$$\frac{C_D \rho_\infty U_\infty^2}{2} \lambda \cos^2 \psi + \frac{\rho F^2}{\lambda} \left(\frac{\lambda}{\delta} - 1 \right) - \zeta = 0 \qquad (32)$$

This is solved for the leading edge thickness, λ which is then combined with Equation 29 to yield V_e, the velocity at which melted titanium spreads over the airfoil in the direction of the streamlines.

K. COMPUTING PROCEDURES

In general, the program proceeds through several main functional areas for each time increment in the simulation.

These function areas are as follows:

1. Evaluation of temperature field in solid airfoil,
2. Test for occurence of ignition,
3. Analysis of flowing melt processes,
4. Evaluation of spread of melt-covered region,
5. Evaluation of change in airfoil geometry due to melting, and
6. Return to (1).

Figure 12 shows the operational flow and required conditional transfers. Logic diagrams for the various operational blocks are expanded in Reference 8.

L. COMPARISON WITH TEST DATA

Figure 13 shows the comparison of simulation results with photographic data from the combustion test of an uncambered airfoil of Ti 8-1-1. The specimen has a leading edge thickness of 0.012 inch, a midchord thickness of 0.050 inch, and a chord of 1.00 inch. The combustion test was performed with at an air temperature of 800°F and pressure of 90 psia, with a velocity of 400 ft/sec.

While not identical in appearance, the model simulation displays the basic characteristics of the experimental data.

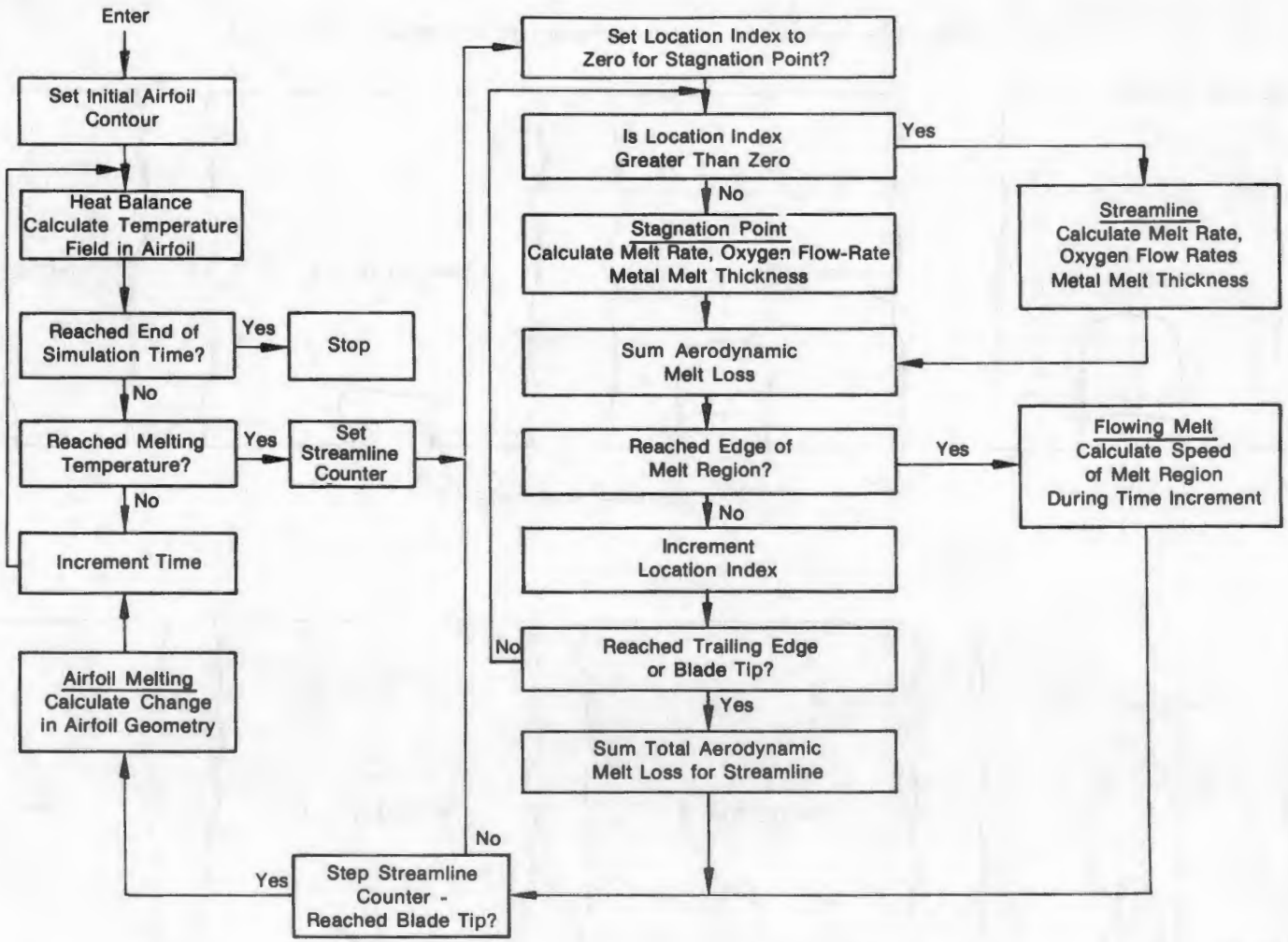

Figure 12. Generalized Combustion Program Logic

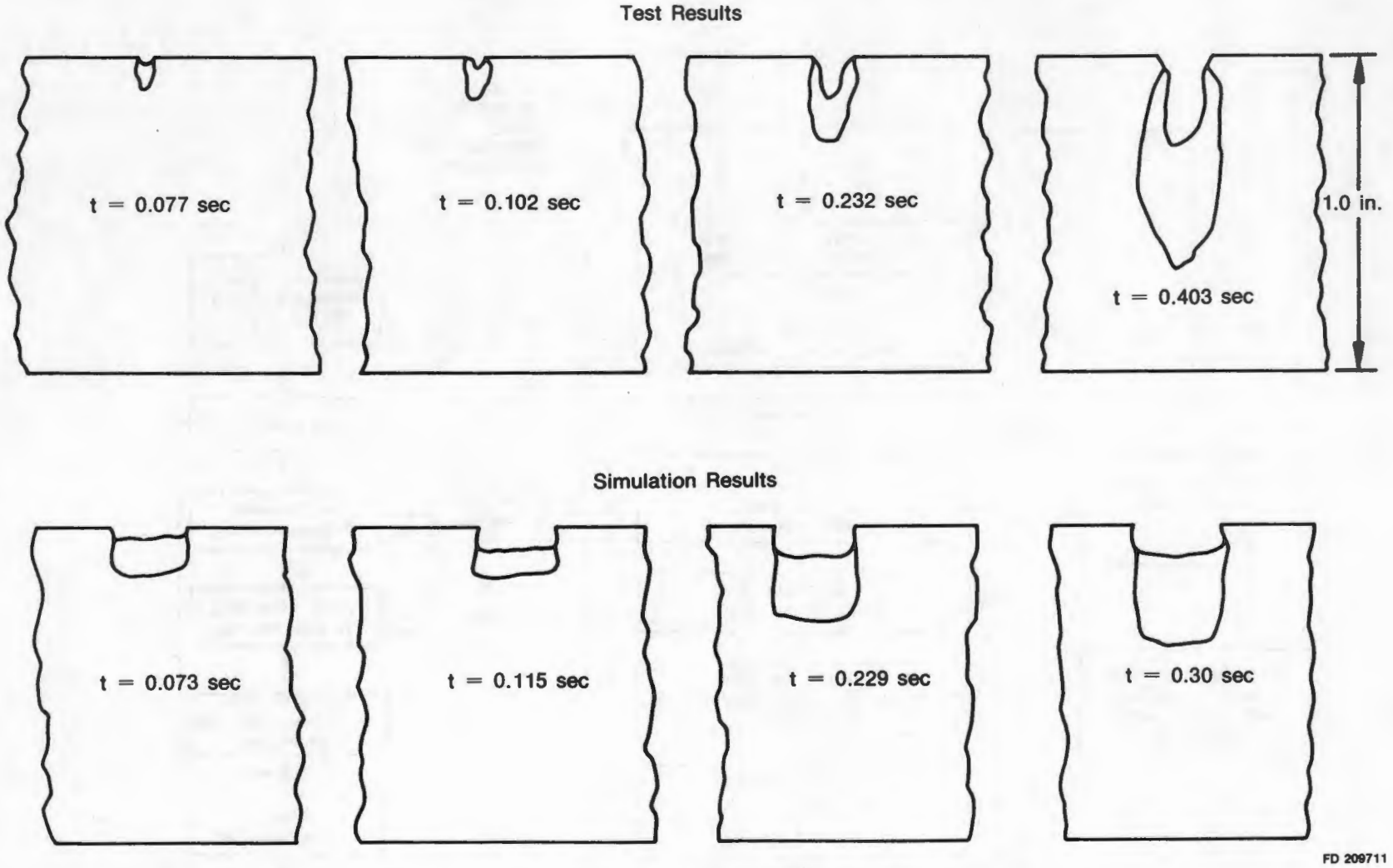

Figure 13. Comparison of Combustion Test and Model Simulation

SUMMARY OF RESULTS

The self-sustained combustion of a selected titanium alloy (Ti-8Al-1Mo-1V), has been investigated over a range of temperatures, pressures and flow-velocities encompassing the typical gas turbine engine compressor environment.

A basic analytical model has been developed to simulate the ignition and self-sustained combustion of stationary titanium alloy airfoils in gas turbine environments, and the model has been programmed for computer evaluation. Preliminary results with the model indicate that it is generally in good agreement with the test data in predicting the lower limits of self-sustained combustion and in simulating liquid metal flow; however, some details of the model required further development to provide a predictive technique generally applicable to a wide range of gas turbine engine environments.

The analytical model was further generalized and programmed for computer solution to include the effects of centrifugal body forces on liquid metal flow and propagation, thus extending its application to analysis of compressor stators and rotors. Also, to provide better agreement with observed experimental behavior, liquid flow models were expanded to include aerodynamic coupling mechanisms controlling loss of melt from the surface, and physical property models were developed to include the effect of absorbed oxygen on thermodynamic and transport properties.

ACKNOWLEDGMENT

Development of the analytical models described in this paper was performed under two subsequent Air Force programs, Contract F33615-76-C-5041 (AFML) and Contract F33615-79-C-2003 (AFAPL).

LIST OF SYMBOLS

Notation

C_D	=	aerodynamic drag coefficient
C_F	=	coefficient of friction
C_p	=	specific heat
D	=	oxygen diffusivity in metal
$\overline{F}$	=	melt flow vector
F	=	melt flow scalar
f	=	chordwise component of melt flow
g	=	oxygen convective flow in melt
h	=	radial component of melt flow
H	=	enthalpy of metal
H_{ox}	=	heat of reaction per unit mass of oxygen
H_{sl}	=	latent heat of fusion
i,j	=	unit vectors in chordwise and radial directions
M	=	mass of oxygen bonded on surface
$\dot{m}_o$	=	oxygen mass flux
n	=	direction normal to surface
$\overline{q}_s$, q_s	=	surface heat flux vector, scalar
$\overline{q}_k$, q_k	=	internal conduction vector, scalar
R	=	leading edge aspect ratio
$\overline{R}$	=	radius to mid-span of blade
S,J	=	streamline position and location indices
s	=	distance along streamline
t	=	time
T	=	temperature in melted metal
T_g	=	gas temperature
T_m	=	melting temperature
T_n	=	node temperature
U	=	melting velocity of surface
U_∞	=	free-stream air velocity
u, v	=	chordwise and radial velocity components (melt)
$\overline{V}$, V	=	liquid metal velocity vector, scalar
W	=	width of streamline
X,Y,Z	=	chordwise, normal, radial coordinate system
β	=	centrifugal body force per volume
γ	=	leading edge yaw angle
Γ	=	mass transport ratio (Eq. 20)
δ	=	liquid metal film thickness
Δ	=	local thickness of airfoil
ζ	=	component of surface tension parallel to surface
η	=	dimensionless distance from solid surface
λ	=	thickness of liquid metal leading edge
μ	=	dynamic viscosity of liquid metal
ξ	=	fraction of melt flow loss from surface
ρ	=	metal density
ρ_a	=	air density
τ	=	aerodynamic shear stress in chordwise direction
τ_o	=	aerodynamic shear stress in radial direction
ϕ	=	local oxygen mass-fraction in liquid metal
ϕ	=	bulk (mean) oxygen mass-fraction in liquid metal
ψ	=	streamline angle relative to chord
ω	=	rotational speed of blade

LIST OF SYMBOLS

Notation

Subscripts

$_s$ = solid
$_l$ = liquid
$_i$ = liquid-solid interface
$_o$ = liquid metal-air interface

REFERENCES

1. "Ignition and Self-Sustained Combustion of Titanium Alloys," Third DoD Laser Effects Vulnerability and Countermeasures Meeting, 19 July 1977, San Diego, CA (with B. A. Manty, S. R. Lyon, and C. W. Elrod).

2. "Final Report of Titanium Combustion Research Program," AFML-TR-79-4001, Air Force Materials Laboratory, WPAFB, Ohio, March 1979.

3. Schofield, T. H. and A. E. Bacon, *Journal of the Institute* of Metals, Vol. 84 (1955-56), p. 47.

4. "Casting Properties of Titanium Alloys," O. N. Magnitskiy, 1968, Translation by Foreign Technology Division, WPAFB, 1970.

5. Orr, Clyde, Jr., and Dalla Valle, J. M., "Heat Transfer Properties of Liquid-Solid Suspensions, *"Chem. Eng. Prog. Symposium No. 9*, 1954.

6. Roe, W. P., H. R. Palmer, and W. R. Opie, "Diffusion of Oxygen in Alpha and Beta Titanium," Transactions of the ASM, Vol. 52 (1960) pp. 191-200.

7. Touloukian, Y. S., *Metallic Elements and Their Alloys*, TPRC Databook, Vol. 1, Purdue Research Foundation, Lafayette, Indiana, 1964.

8. "Titanium Airfoil Combustion Program User's Manual for Deck CCD 1152-O.O," AFML-TR-79-4001, Air Force Materials Laboratory, WPAFB, Ohio, March 1979.